Validation of the actuator line and disc techniques using the New MEXICO measurements

S. Sarmast[1], W.Z. Shen[2], W.J. Zhu[2], R.F. Mikkelsen[2], S.P. Breton[1], S. Ivanell[1,3]

[1]Uppsala University, Wind Energy Section, Campus Gotland, 621 67 Visby, Sweden
[2]Wind Energy Department, Technical University of Denmark, 2800 Lyngby, Denmark
[3]KTH Mechanics, 100 44 Stockholm, Sweden

E-mail: sasan.sarmast@geo.uu.se

Abstract.

Actuator line and disc techniques are employed to analyse the wake obtained in the New MEXICO wind turbine experiment. The New MEXICO measurement campaign done in 2014 is a follow-up to the MEXICO campaign, which was completed in 2006. Three flow configurations in axial flow condition are simulated and both computed loads and velocity fields around the rotor are compared with detailed PIV measurements. The comparisons show that the computed loadings are generally in agreement with the measurements under the rotor's design condition. Both actuator approaches under-predicted the loading in the inboard part of blade in stall condition as only 2D airfoil data were used in the simulations. The predicted wake velocities generally agree well with the PIV measurements.

In the experiment, PIV measurements are also provided close to the hub and nacelle. To study the effect of hub and nacelle, numerical simulations are performed both in the presence and absence of the hub geometry. This study shows that the large hub used in the experiment has only small effects on overall wake behaviour.

1. Introduction

The growth of wind energy around the world is associated with increased research efforts to improve the aerodynamics of wind turbine designs and to develop more reliable prediction tools. In order to test and validate those new tools, there is a need for well-documented experimental databases. Despite the high cost of wind tunnel measurements, limited well-documented full scale investigations have been performed including the NREL Phase VI rotor measurements in the NASA Ames wind tunnel [1]. The MEXICO (Model Experiments in Controlled Conditions) experimental rotor was tested in the 9.5×9.5 m^2 LLF (Large Scale Low Speed Facility) of the German Dutch Wind tunnel (DNW) [2]. This model rotor is three-bladed and has a diameter of 4.5 m. The rotor blade is composed of a cylinder from 0% to 4.4% span, the DU91-W2-250 airfoil from 11.8% to 40% span, the RISØ A1-21 airfoil from 50% to 62% span and the NACA64-418 from 72% to 100% span with three transitional zones between the airfoils. The turbine was mounted on the wind tunnel 6 components balance, where total forces and moments were measured. Detailed aerodynamic measurements in particular pressure and flow field measurements are carried out. The flow field around the rotor, inflow and near wake were measured using the Particle Image Velocimetry (PIV) technique. The obtained experimental

Table 1. Rotor specifications

Rotor	blade length, r [m]	hub size, h [m]	h/(h+r)
NREL 5-MW baseline [5]	61.5	1.5	2.4%
Vestas V90 3-MW [6]	44	1	2.2%
Siemens SWT-2.3-93 [7]	45	1.5	3.2%
Tjæreborg Wind Turbine [8]	29.1	1.45	2.4%
NREL Phase VI Experiment [9]	5.02	0.508	10.9%
New Mexico Experiment	2.040	0.27	12.0%
NTNU Experiment [10]	0.402	0.045	10.0%

data were used by the wind energy research community to validate their prediction tools [3]. In summer 2014, the MEXICO project was revisited [4], and this time more detailed measurements were conducted, including the flow fields close to the hub and noise measurements.

In small scale rotor experiments, the rotor has a large hub geometry in comparison to typical wind turbines. Table 1 provides an estimation of the hub size for both experimental and real wind turbines. It is difficult to keep the same hub to rotor radius ratio for experimental rotor as it is not always possible to downscale all the components inside the hub and nacelle. Those components include different measurement instruments, pitching mechanisms, hub components and main shaft which should fit in the limited space. The presence of hub and tower geometry are usually neglected in numerical simulations [11–13]. The present study focuses on the validation of the actuator line and disc approaches as well as studying the the flow around the hub and nacelle in the near wake.

2. Numerical method and setup

The numerical simulations are performed using the multi-block finite volume Navier–Stokes solver EllipSys3D in conjunction with the actuator line and disc techniques [19]. In the actuator disc and line approaches, the presence of the rotor is replaced by body forces distributed over a disc or along the 3 blade lines, respectively. The body forces represent the aerodynamic loadings on the wind turbine blades. At each actuator point, the force is smeared among neighboring nodes with a three-dimensional Gaussian smearing function[15]. The smearing parameter (ϵ) is

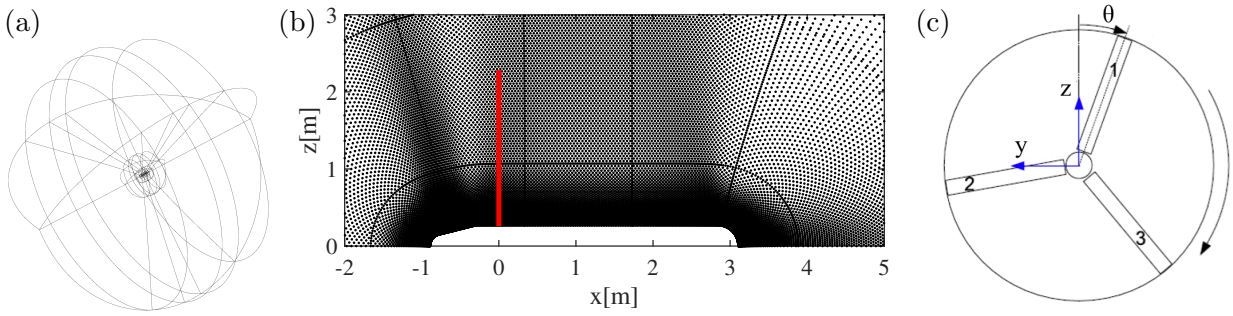

Figure 1. (a) Three dimensional mesh where the curves are block boundaries, (b) mesh distribution around the rotor in the second grid level setup. The rotor is positioned at $x = 0$. (c) Schematic front view of the rotor, θ denotes the rotor azimuthal angle.

chosen to be $\epsilon = 2.5dr$ where dr is the local grid (actuator) resolution along the blade. The 2D airfoil coefficients are provided by Boorsma *et al.* [4] which are DU91-W2-250 at $Re_c = 0.5 \times 10^6$ (rough), RISØ A1-21at $Re_c = 1.6 \times 10^6$ (rough) and NACA64-418 at $Re_c = 0.7 \times 10^6$ (clean). Here, Re_c is the chord based Reynolds number. The advantage of both actuator methods is that they avoid resolving the boundary layer over the blades and thus more grid points can be utilized to capture the details of near wake. The actuator line and disc methods are implemented into the EllipSys3D code, developed by Michelsen [16] and Sørensen [17]. Large-Eddy Simulation (LES) is employed, in which the large scales are resolved and the small scales are modeled by the eddy viscosity based sub-grid scale model by Ta Phouc [18].

The computations are performed using two computational grid configurations which consider the presence and absence of the hub and nacelle geometry. The first setup, where the geometry of hub and nacelle is not considered is a structured Cartesian grid with 45 blocks and approximately 11.8 million grid points in a domain of size $[-16R, 16R] \times [-16R, 16R] \times [-16R, 16R]$ with the finest cell size equal to $R/40$. R is the rotor radius. In both actuator line and disc simulations each blade is presented by 41 actuator points. In this setup the presence of the hub is introduced using forces in the inboard part of the rotor, $r \leq 0.27m$. This is done by simply assuming zero lift coefficient $C_l = 0$ and the drag coefficient produced by a cylinder to be $C_d \approx 1.2$.

The second setup is a structured grid containing five blocks in both the radial and axial directions and three blocks in the azimuthal direction. The mesh extends to $26R$ in all three directions. This results in a total number of 75 blocks and 19.66 million grid points. The geometry of the hub and nacelle are reproduced based on the experimental model and it can be described as a cylinder with a cone shaped front and spherical end, see Figure 1. Solid walls are utilized at the nacelle surface. Sufficient grid points close to the surface are considered in order to resolve the boundary layer. The first grid point is located at approximately $2 \times 10^{-4}R$ which results in $y^+ \approx 4 - 5$. Considering the boundary conditions, the velocity is assumed to be uniform in the axial direction. A convective outflow boundary condition is used at the outlet. No initial turbulence is considered as the measured turbulence intensity in the wind tunnel is very small and the wind tunnel geometry is not included as previous investigation by Shen *et al.* [11] showed that the tunnel effects are not significant.

3. Results and discussions

The flows with the incoming wind velocities of 10, 15 and 24 m/s past the MEXICO rotor running at a rotational velocity of 425.1 rpm are computed. Axial flow condition is considered and the pitch of the blades are set to be -2.3° (nominal condition). The normal and tangential blade loadings are computed for three incoming wind speeds and reported in Figure 2. The loadings are measured at five points along the span, i.e. 25%, 35%, 60%, 82% and 92%R. Higher loadings are observed by increasing of the incoming velocity. Computed loads are generally in agreement with measurements except in the inboard part of the blade (at the 25% and 35%R positions) for $U = 24$ m/s, where the forces are under-predicted. This indicates an under-prediction of stall and it is caused by the use of the 2D airfoil data suggested in the IEA Task 29 MexNext project in order to make fair comparisons between different numerical approaches. It is possible to achieve better agreement using 3D airfoil corrections [11]. The comparison also shows that the presence of hub has no effect on the loading distributions in the inboard part of the blade.

Figure 3 shows the wake development computed using the actuator line and disc approaches. The wakes simulated by actuator line approach consist of organized tip and root vortices while in actuator disc vortex sheets are developed behind the rotor. The position of tip and root structures are generally in agreement between the two approaches. It is also shown that by introducing the hub the structures formed near the root decay faster due to their interactions with the hub and nacelle.

The computed wake behind the rotor is compared with the detailed PIV data, where the

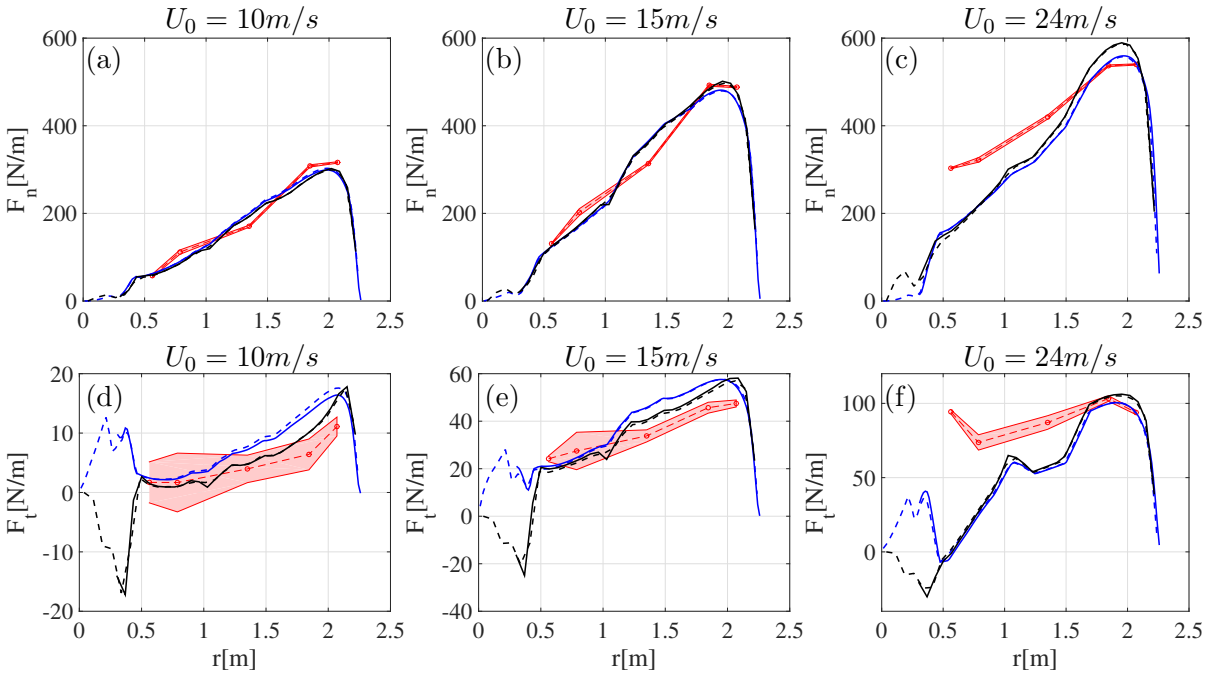

Figure 2. Normal force (Fn) distribution along blade (the force normal to the chord), (a) $U_0 = 10m/s$, (b) $U_0 = 15m/s$ and (c) $U_0 = 24m/s$, and tangential force (Ft) distribution along blade (the force parallel to the chord), (d) $U_0 = 10m/s$, (e) $U_0 = 15m/s$ and (f) $U_0 = 24m/s$: Experiment (○), actuator disc computations with presence of hub (—) and actuator line computations with presence of hub geometry (—). Dashed lines represent the simulations in absence of the hub and nacelle geometry. Red areas show the experimental uncertainties. Similar legends are used in Figures 4-10.

instantaneous velocity fields along various lines (axial, radial and tangential traverses) are extracted for different incoming velocities. Figures 4-6 show the comparisons using the radial traverses before and after the rotor ($x = +0.3m$). The PIV results are obtained in a plane at 9 o'clock when looking downstream at the rotor. The PIV system covers the radial region from r=0.3m to r=2.68m. It is shown that the axial velocities computed with both the actuator line and disc approaches over-predict the PIV measurements at both upstream and downstream from the rotor. Looking at the axial velocities downstream of the rotor, it is possible to detect three regions with different induction velocities which is directly related to the three airfoil profiles used along the blade span. Looking closely at the radial and azimuthal velocities, we can observe that the overall measured trends are captured by the simulations while differences are observed in the inboard part ($r < 1m$), close to the hub. These differences are especially pronounced for the radial velocities upstream of the rotor. It is shown that including the hub improves the agreement. Far upstream of the rotor, the flow is developing only in axial direction with no radial velocity component, while when it reaches the cone-shaped hub, due to the conservation of mass the flow is forced to change its direction which leads to an increase of its radial velocity. The increase in radial velocity can only be captured if the hub geometry is introduced in the simulation.

Axial traverses are used to compare the velocity along the lines in the axial direction. The velocity field is extracted along two lines across the rotor plane at $r = 0.5m$ and $r = 1.5m$ in the horizontal plane at the 9 o'clock position. The PIV measurements cover the axial range between $x = -4.5m$ (upstream) to $x = 5.9m$ (downstream). In Figure 7, three velocity components are

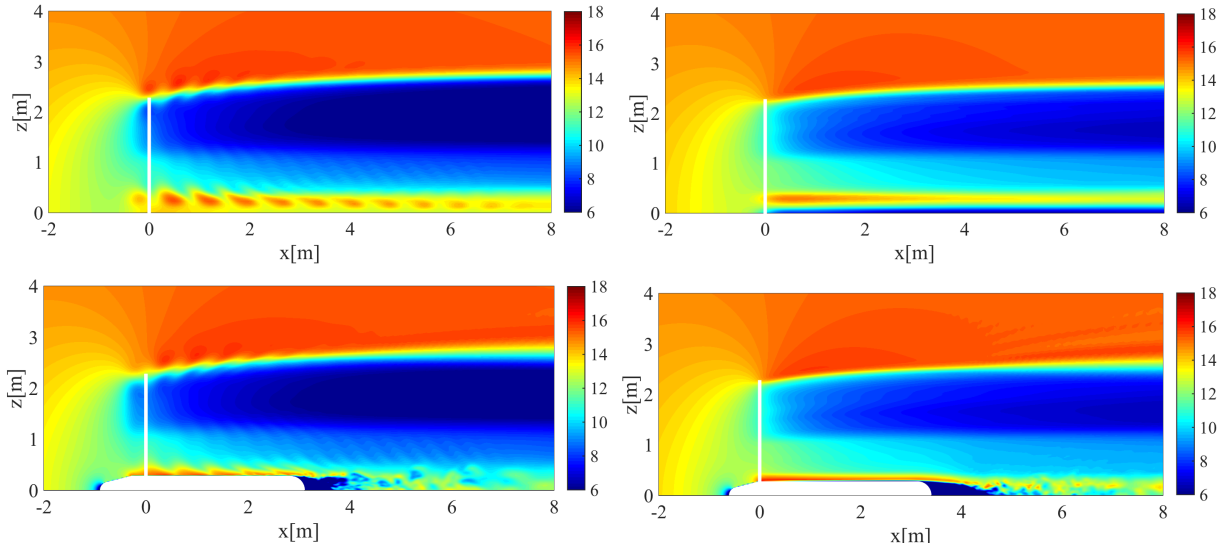

Figure 3. Contours of axial velocity for $U_0 = 15m/s$ inflow computed using actuator line (left) and actuator disc (right) approaches, (top) simulations in the absence of the nacelle and (bottom) simulations with the presence of the nacelle. The blade azimuthal position is set to be $\theta = 60°$.

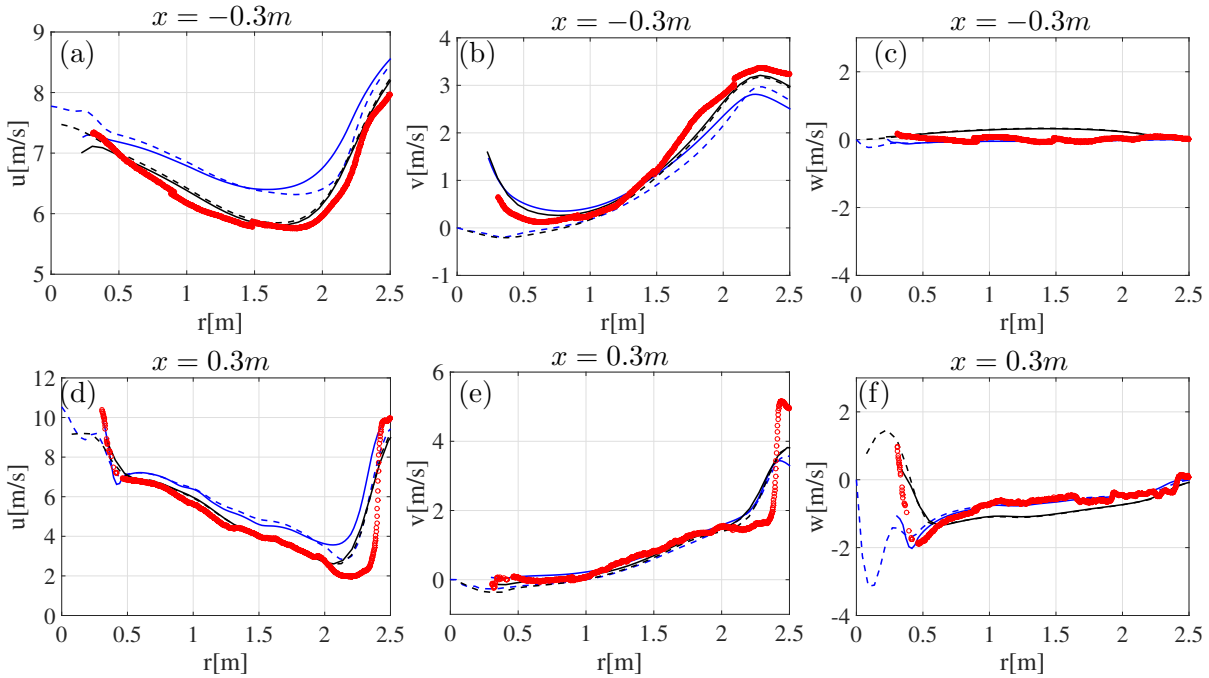

Figure 4. (a) Axial, (b) radial and (c) tangential velocities at $x = -0.3m$ (upstream), (d) axial, (e) radial and (f) tangential velocities at $x = +0.3m$ (downstream) at the 9 o'clock position and a wind speed of $U_0 = 10m/s$. Similar legends as Figure 2 are used here.

compared with the experiments for the incoming velocity of $U_0 = 15m/s$. Oscillations observed in (a-c) profiles are related to the presence of the root vortices while the oscillations in (d-f) are related to the development of the tip vortices in the near wake. In actuator disc simulations, it

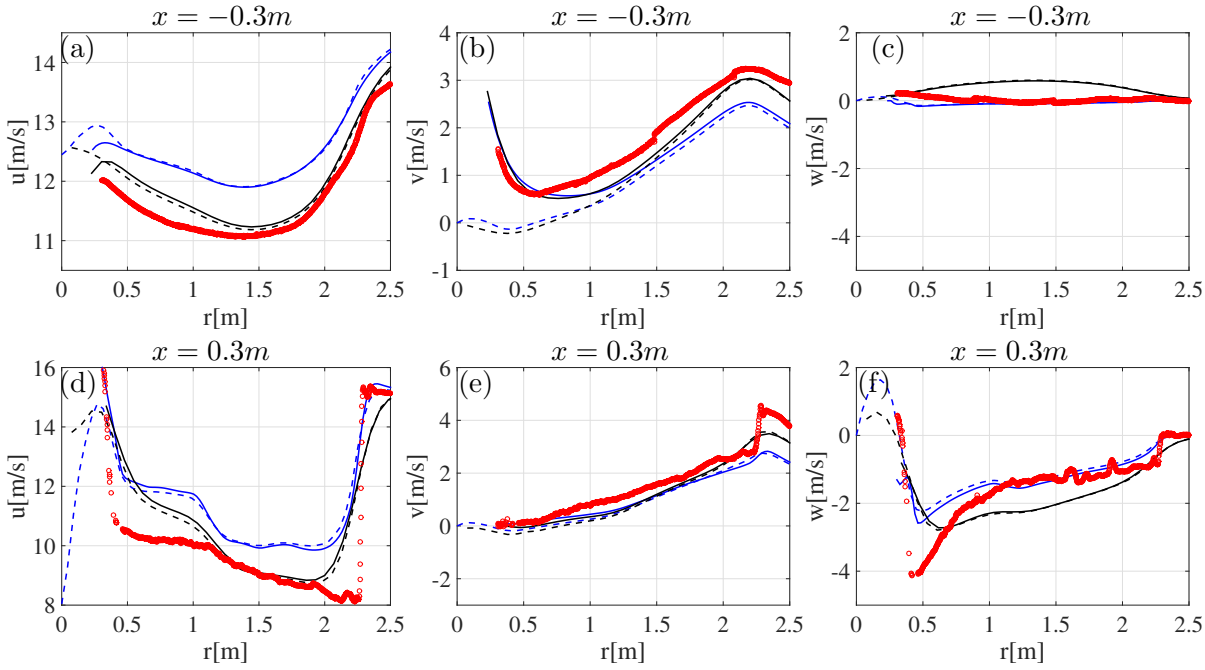

Figure 5. (a) Axial, (b) radial and (c) tangential velocities at $x = -0.3m$ (upstream), (d) axial, (e) radial and (f) tangential velocities at $x = +0.3m$ (downstream) at the 9 o'clock position and a wind speed of $U_0 = 15m/s$. Similar legends as Figure 2 are used here.

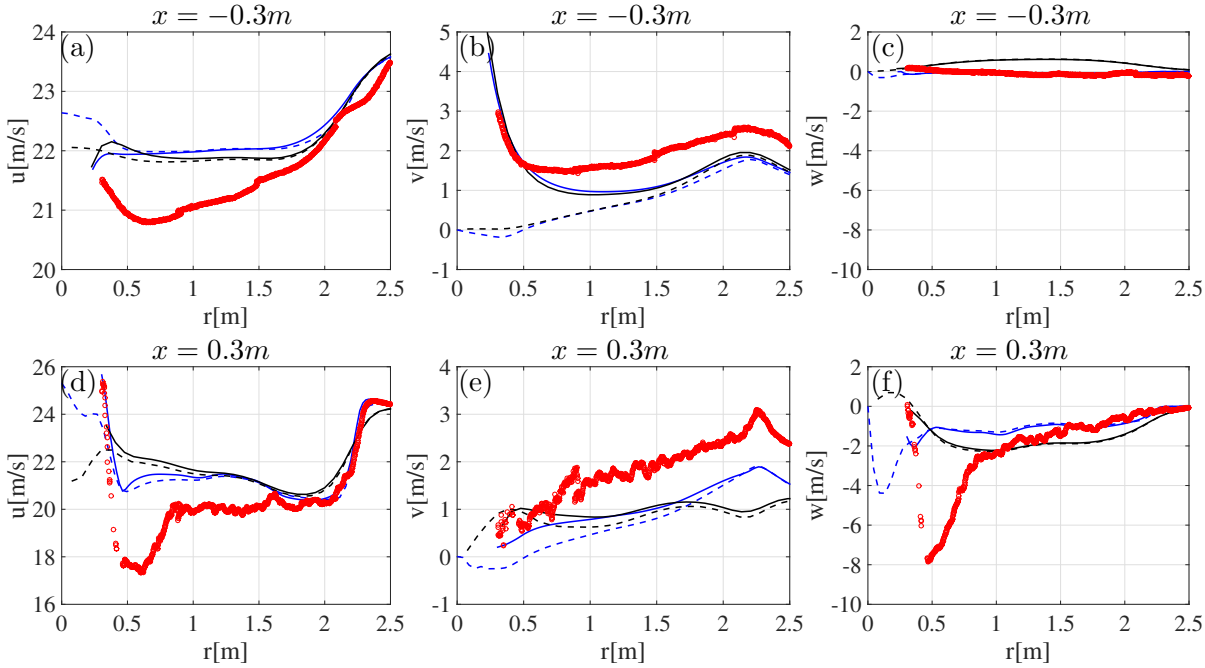

Figure 6. (a) Axial, (b) radial and (c) tangential velocities at $x = -0.3m$ (upstream), (d) axial, (e) radial and (f) tangential velocities at $x = +0.3m$ (downstream) at the 9 o'clock position and a wind speed of $U_0 = 24m/s$. Similar legends as Figure 2 are used here.

is not possible to capture these oscillations as the presence of the rotor is modelled using forces distributed over a disc and this model is not able to simulate tip and root vortices. Comparing the axial velocity, it is shown that both actuator line and disc approaches over-predict the velocity in the inboard part of the blade. A jump is observed close to the rotor using the actuator line method. In the outboard part of the blade, the velocity over-prediction of the actuator disc can be related to the lower local induction. Figure 7(b) shows an increase in the radial velocity close to the rotor $x \approx 0$ which can only be captured if the hub and nacelle geometry are considered.

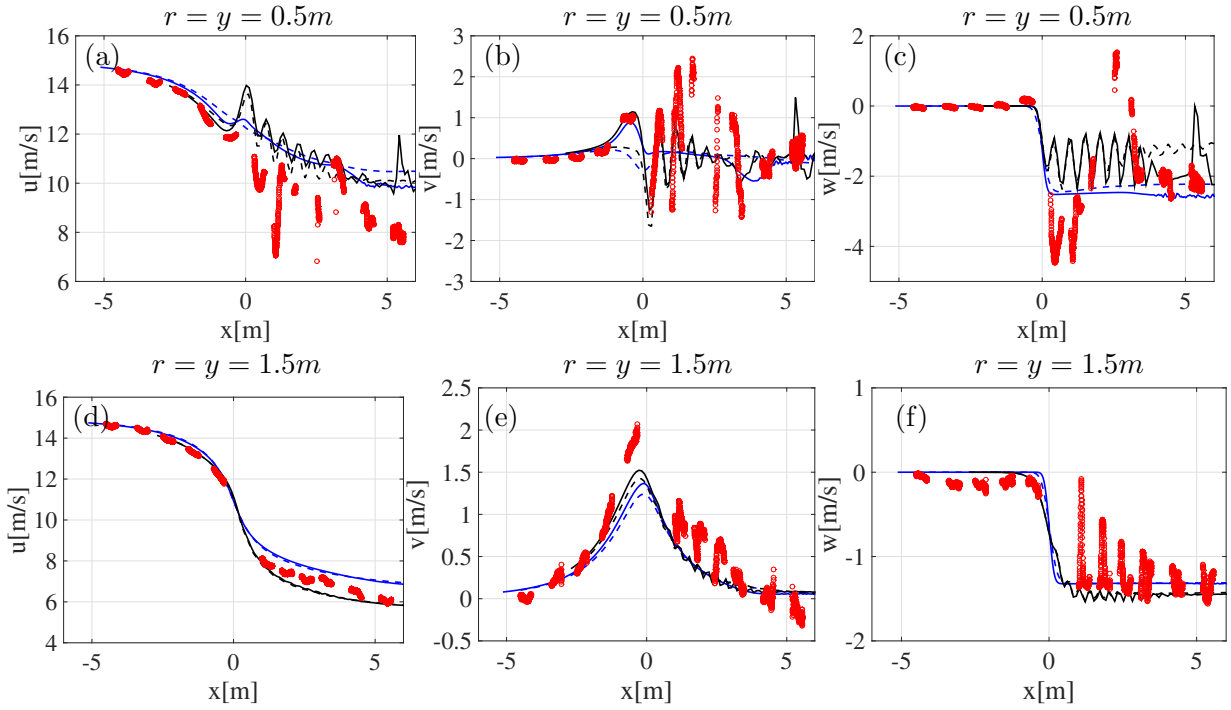

Figure 7. (a) Axial, (b) radial and (c) tangential velocities at $r = y = 0.5m$ (inboard) and (d) axial, (e) radial and (f) tangential velocities at $r = y = 1.5m$ (outboard) in the horizontal plane at the 9 o'clock position and a wind speed of $U_0 = 15m/s$. Similar legends as Figure 2 are used here.

PIV measurements are also obtained at five radial positions, ($r = 0.56$, 0.79, 1.35, 1.85 and $2.07m$) and azimuthal positions ranging between $\theta = 0°$ to $\theta = 120°$. The measurements are performed in the horizontal plane at the 9 o'clock position of the rotor plane. The comparison of velocity components for $r = 0.56m$ (in-board), $r = 1.35m$ and $r = 2.07m$ (outboard) are shown in Figures 8-10. Simulating the flow using the actuator disc approach shows that the velocity components are constant for different azimuthal positions. This azimuthal consistency is due to the axis-symmetry properties of the actuator disc approach. Introduction of the hub and nacelle geometry improves the agreement close to the rotor. This comparison shows that the actuator line simulations are capable of capturing the details of the flow, while the actuator disc approach is able to provide an averaged approximation of the flow behaviour.

4. Conclusions

The actuator disc and line approaches were tested against the detailed measurements performed in the New MEXICO project. Generally, good agreement between the computations and the experiments is seen for the loadings along the blade. The computations agree well with the measured velocity profiles in the axial, radial and azimuthal directions. This study shows that

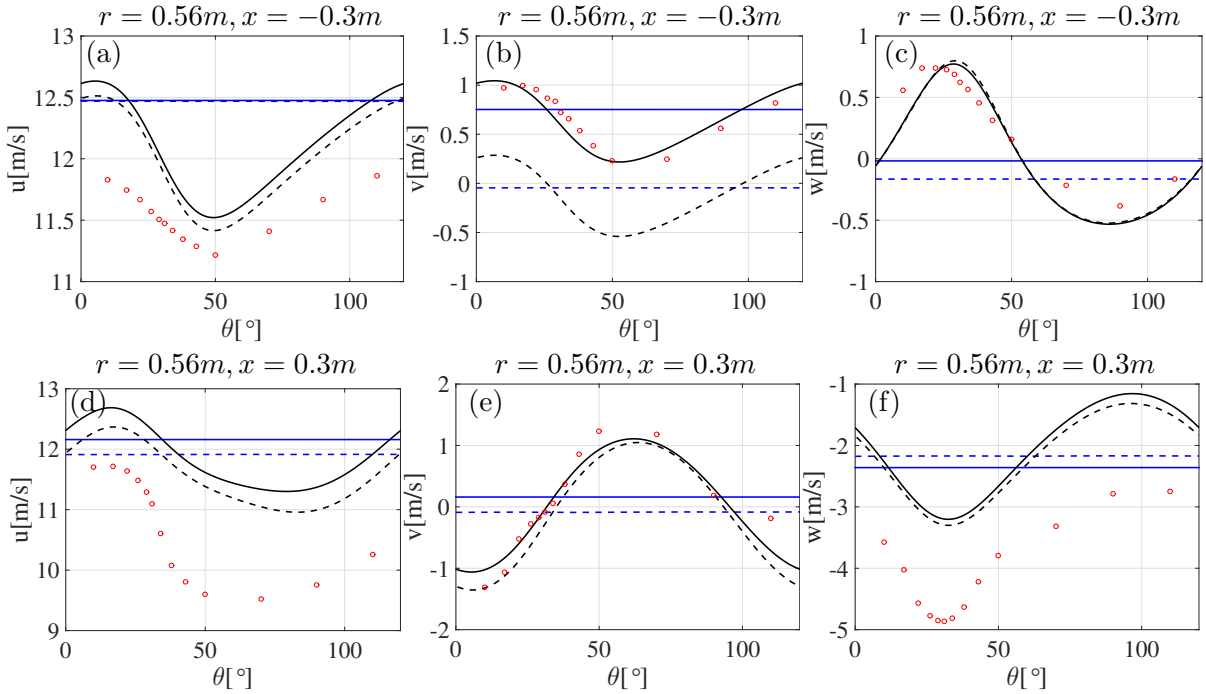

Figure 8. (a) Axial, (b) radial and (c) tangential velocities are computed at the $x = -0.3m$ upstream position and (d-f) are the velocities computed at $x = +0.3m$ downstream of the rotor at $r = 0.56m$ and an incoming wind speed of $U_0 = 15m/s$. Similar legends as Figure 2 are used here.

the flow around the hub and nacelle geometry doesn't have any effect on the blade loadings. It was also found that it is important to introduce the hub and nacelle geometry in order to match the measured velocities close to the hub and nacelle ($r < 1m$) but it can also be concluded that considering the hub and nacelle has a negligible effect on overall wake behaviour.

Acknowledgments
This work was supported by the Energy Technology Development and Demonstration Program (EUDP2014, J. nr. 64014-0543) under the Danish Energy Agency. The simulations were performed on resources provided by the Swedish National Infrastructure for Computing (SNIC) within the project SNIC 2015/10-24. The authors wish to thank the international partners for their collaborations in the MexNext project coordinated by Energy research Centre of the Netherlands (ECN), within the framework of IEA Task 29.

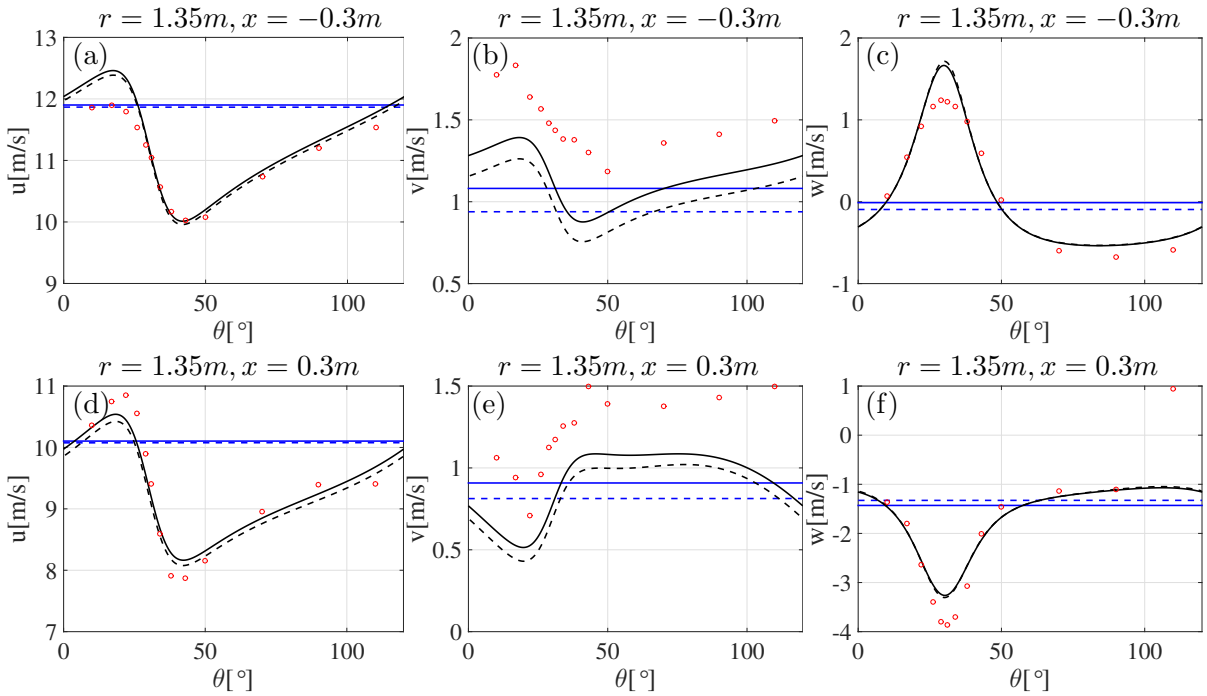

Figure 9. (a) Axial, (b) radial and (c) tangential velocities are computed at the $x = -0.3m$ upstream position and (d-f) are the velocities computed at $x = +0.3m$ downstream of the rotor at $r = 1.35m$ and an incoming wind speed of $U_0 = 15m/s$. Similar legends as Figure 2 are used here.

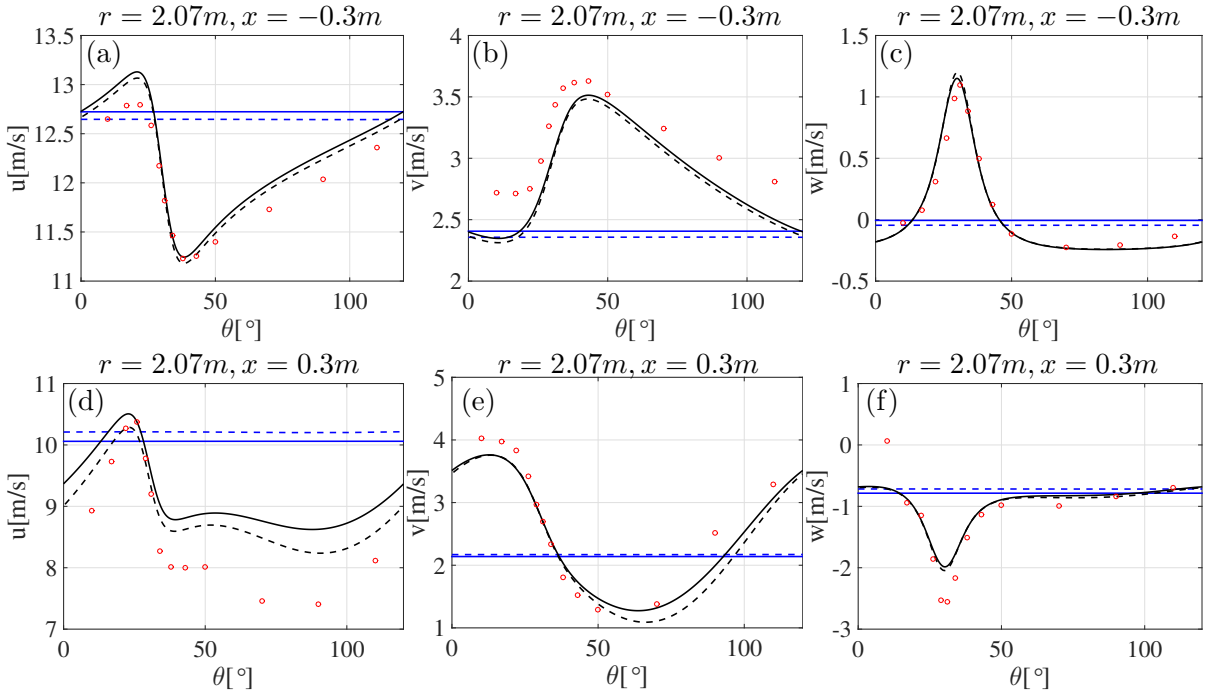

Figure 10. (a) Axial, (b) radial and (c) tangential velocities are computed at the $x = -0.3m$ upstream position and (d-f) are the velocities computed at $x = +0.3m$ downstream of the rotor at $r = 2.07m$ and an incoming wind speed of $U_0 = 15m/s$. Similar legends as Figure 2 are used here.

References

[1] Simms D A, Schreck S, Hand M and Fingersh L 2001 *NREL unsteady aerodynamics experiment in the NASA-Ames wind tunnel: a comparison of predictions to measurements* (National Renewable Energy Laboratory Golden, CO, USA)

[2] Snel H, Schepers J and Montgomerie B 2007 *Journal of Physics: Conference Series* vol 75 (IOP Publishing) p 012014

[3] Schepers J, Boorsma K, Cho T, Gomez-Iradi S, Schaffarczyk P, Jeromin A, Shen W Z, Lutz T, Meister K, Stoevesandt B *et al.* 2012

[4] Boorsma K and Schepers J 2014 New mexico experiment: Preliminary overview with initial validation Tech. Rep. ECN-E–14-048 ECN

[5] Jonkman J M, Butterfield S, Musial W and Scott G 2009 Definition of a 5-mw reference wind turbine for offshore system development

[6] Vestas G S 2011 V90-3.0 mw

[7] Siemens A 2009 *Germany: Siemens AG*

[8] Øye S 1990 *VK–184, Dept. of Fluid Mechanics, Technical University of Denmark: Lyngby*

[9] Hand M M, Simms D, Fingersh L, Jager D, Cotrell J, Schreck S and Larwood S 2001 *Unsteady aerodynamics experiment phase VI: wind tunnel test configurations and available data campaigns* (National Renewable Energy Laboratory Golden, Colorado, USA)

[10] Krogstad P Å and Adaramola M S 2012 *Wind Energy* **15** 743–756

[11] Shen W Z, Zhu W J and Sørensen J N 2012 *Wind Energy* **15** 811–825

[12] Nilsson K, Shen W Z, Sørensen J N, Breton S P and Ivanell S 2015 *Wind Energy* **18** 499–514

[13] Sørensen N N, Bechmann A, Réthoré P E and Zahle F 2014 *Wind Energy* **17** 75–86

[14] Sørensen J N and Shen W Z 2002 *J. Fluid Eng.* **124** 393–399

[15] Mikkelsen R 2003 *Actuator Disc Methods Applied to Wind Turbines* Ph.D. thesis Dept. of Fluid Mech., Technical University of Denmark, DTU

[16] Michelsen J A 1994 Block structured multigrid solution of 2D and 3D elliptic PDE's Tech. Rep. AFM 94-06 Dept. of Fluid Mech., Technical University of Denmark, DTU

[17] Sørensen N N 1995 *General purpose flow solver applied to flow over hills* Ph.D. thesis Risø National Laboratory Roskilde

[18] Ta Phuoc L 1994 *Proc. of the DRET conference: 'Aérodynamique Instationnaire Turbulents - Aspects Numériques et Expérimentaux*

[19] Sørensen J and Shen W 2002 *Journal of fluids engineering* **124** 393–399